

Surface oxidation effect on the electrical behaviour of $\text{Bi}_2\text{Te}_2\text{Se}$ nanoplatelets

This content has been downloaded from IOPscience. Please scroll down to see the full text.

2016 Nanotechnology 27 285201

(<http://iopscience.iop.org/0957-4484/27/28/285201>)

View [the table of contents for this issue](#), or go to the [journal homepage](#) for more

Download details:

IP Address: 207.162.240.147

This content was downloaded on 09/09/2016 at 16:26

Please note that [terms and conditions apply](#).

You may also be interested in:

[Raman and interband optical spectra of epitaxial layers of the topological insulators \$\text{Bi}_2\text{Te}_3\$ and \$\text{Bi}_2\text{Se}_3\$ on \$\text{BaF}_2\$ substrates](#)

J Humlíek, D Hemzal, A Dubroka et al.

[Oxygen Plasma Functioning of Charge Carrier Density in Zinc Oxide Thin-Film Transistors](#)

Min-Ching Chu, Jagan Singh Meena, Po-Tsun Liu et al.

[Charge puddles in a completely compensated topological insulator](#)

C W Rischau, A Ubaldini, E Giannini et al.

[Synthesis and field emission properties of topological insulator \$\text{Bi}_2\text{Se}_3\$ nanoflake arrays](#)

Yuan Yan, Zhi-Min Liao, Feng Yu et al.

[Evidence for topological surface states in metallic single crystals of \$\text{Bi}_2\text{Te}_3\$](#)

Sourabh Barua, K P Rajeev and Anjan K Gupta

[Electrostatic field effects on three-dimensional topological insulators](#)

Yang Wen-Min, Lin Chao-Jing, Liao Jian et al.

[Shubnikov–de Haas oscillations in n and p type \$\text{Bi}_2\text{Se}_3\$ flakes](#)

Hongchao Liu, Shiguang Liu, Ya Yi et al.

Surface oxidation effect on the electrical behaviour of $\text{Bi}_2\text{Te}_2\text{Se}$ nanoplatelets

Pascal Gehring^{1,3}, Frieder B Reusch¹, Soudabeh S Mashhadi¹, Marko Burghard¹ and Klaus Kern^{1,2}

¹Max Planck Institute for Solid State Research, Heisenbergstrasse 1, D-70569 Stuttgart, Germany

²Institut de Physique de la Matière Condensée, Ecole Polytechnique Fédérale de Lausanne, CH-1015 Lausanne, Switzerland

E-mail: pascal.gehring@materials.ox.ac.uk

Received 10 February 2016, revised 9 May 2016

Accepted for publication 17 May 2016

Published 3 June 2016



CrossMark

Abstract

Charge transport in topological insulators is notably influenced by moisture and air in the surrounding environment. At present, however, little is known about the detailed composition of the oxidized surface and its impact on the electrical characteristics of these materials. Here, we investigate the surface oxide formation on the topological insulator $\text{Bi}_2\text{Te}_2\text{Se}$ (BTS) and how this affects its electrical behavior. While ambient exposure of BTS nanoplatelets predominantly creates surface hydroxyl groups, oxygen plasma treatment yields a compact, few-nanometer thick surface oxide layer. The plasma causes p-type doping, accompanied by a decrease of the effective platelet thickness, the interplay of which is manifested in a resistance maximum as a function of plasma treatment time. It is furthermore demonstrated that the structural integrity of the plasma-derived surface oxide is sufficient to enable its use as a gate insulator layer in combination with a top gate.

 Online supplementary data available from stacks.iop.org/NANO/27/285201/mmedia

Keywords: topological insulator, field-effect transistor, surface oxidation

(Some figures may appear in colour only in the online journal)

1. Introduction

Three-dimensional topological insulators (TIs) are insulators in the bulk with metallic, linear dispersing surface states. These surface states consist of spin-polarized Dirac fermions, which are protected by time-reversal symmetry and spin-orbit interaction, rendering them insensitive to non-magnetic surface perturbations [1, 2]. The existence of TI surface states has been experimentally proven by angle-resolved photoemission spectroscopy for various types of materials, including bismuth chalcogenides [3, 4]. A well-investigated compound among the latter is bismuth selenide (Bi_2Se_3), which has a single Dirac cone combined with a bulk band gap of approximately 0.3 eV [5].

By contrast, electrical transport studies have been considerably less successful in revealing the charge carriers in TI surface states. A major hurdle arises from pronounced doping due to point defects, which leads to simultaneous contributions from bulk and surface carrier transport [6]. The situation is further complicated by the sensitivity of TI surfaces against oxidation. While the Bi_2Se_3 surface has been reported to be relatively inert to oxidation by individual adsorbed gases [7], notable oxidation occurs under ambient conditions in the presence of both water and oxygen [8]. Surface oxidation of Bi_2Se_3 can induce significant charge transfer processes, as concluded from second harmonic generation experiments [9]. The formation of surface oxides has been documented to influence the charge transport in thin Bi_2Se_3 sheets [10]. However, despite these clear indications of the relevance of surface oxidation of bismuth-based TIs, only little is known regarding the formation kinetics and structural morphology of

³ Current address: Department of Materials, University of Oxford, Oxford OX1 3PH, UK.

the surface oxide layer, as well as its effect on the charge transport properties of these compounds.

In this letter, we present experiments monitoring the surface oxidation of bismuth telluride selenide $\text{Bi}_2\text{Te}_2\text{Se}$ (BTS), a TI with a relatively large contribution of surface state currents owing to the suppression of intrinsic defects [11]. Surface-related effects like pronounced weak antilocalisation [13], Shubnikov–de Haas oscillations [21] and spin-polarised currents [22] have been observed in BTS nanoplatelets. Like other bismuth chalcogenides, BTS has been documented to undergo sizable surface oxidation upon air exposure [12]. Here, we trace the time evolution of the surface oxide thickness on ultrathin BTS nanoplatelets subjected to two different types of treatments, specifically exposure to ambient and oxygen plasma treatment. On this basis, we furthermore systematically explore the electrical resistivity, carrier mobility and carrier concentration of the samples in dependence of the oxygen plasma treatment extent.

2. Experimental section

2.1. Material synthesis

The BTS nanoplatelets were grown by a previously described vapor–solid process [13]. In a typical growth experiment, 260 mg of Bi_2Se_3 were put in the hot zone (where $T = 582^\circ\text{C}$) of a 60 cm long horizontal tube furnace equipped with a 2.5 cm wide quartz tube. In addition, 350 mg of Bi_2Te_3 were placed 6 cm away ($T = 560^\circ\text{C}$) from the Bi_2Se_3 source towards the colder zone of the furnace. The growth substrates ($4\text{ mm} \times 4\text{ mm}$ Si covered with 300 nm of SiO_x) were placed in the downstream zone of the furnace about 10–14 cm away from the Bi_2Se_3 source material ($T_{\text{substrate}} = 490^\circ\text{C}$ – 480°C). Using an Ar gas flow of 150 sccm, a pressure of 80 mbar, a growth time of 1–5 min, and a growth substrate temperature of $\sim 480^\circ\text{C}$, BTS nanoplatelets with a lateral size of several μm and thickness down to 5 nm were obtained. In this study we investigated platelets with thickness values below 20 nm.

Oxygen plasma treatment was performed with a TePla 100e, Microwave plasma system.

2.2. Material characterisation

The thickness of the nanoplatelets was determined using an atomic force microscope (AFM, Bruker Dimension Icon) in tapping mode under ambient conditions. Heights were measured on at least three different positions of a nanoplate using the section or step tool, and then the mean value and the standard deviation (shown as error bars in figures 1 and 2) were calculated. X-ray photoelectron spectroscopy (XPS) of the BTS nanoplatelets before and after O_2 plasma treatment was performed with a monochromatized Al K-alpha XPS (Kratis Analytical AXIS ultra). Raman measurements were carried out under ambient conditions using a confocal Raman setup (NT-MDT NTEGRA SPECTRA) with a laser wavelength of 633 nm (spot size $\approx 500\text{ nm}$). The reflected light was analyzed by a Raman spectrometer with a peak-to-peak

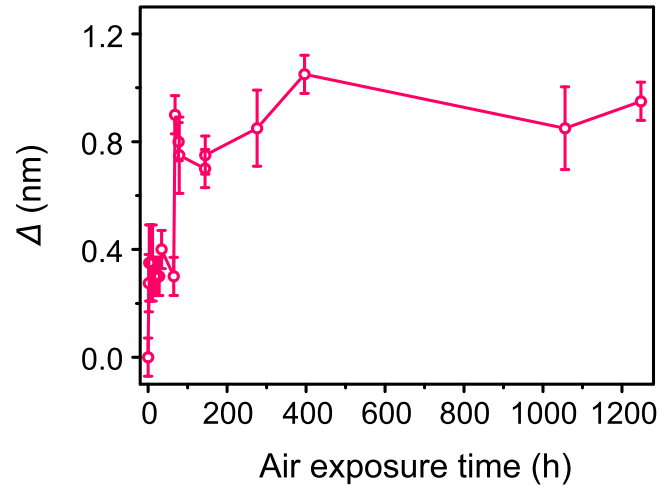


Figure 1. Evolution of the thickness of a BTS nanoplatelet upon exposure to ambient conditions. The thickness values are extracted from atomic force microscopy (AFM) height profiles.

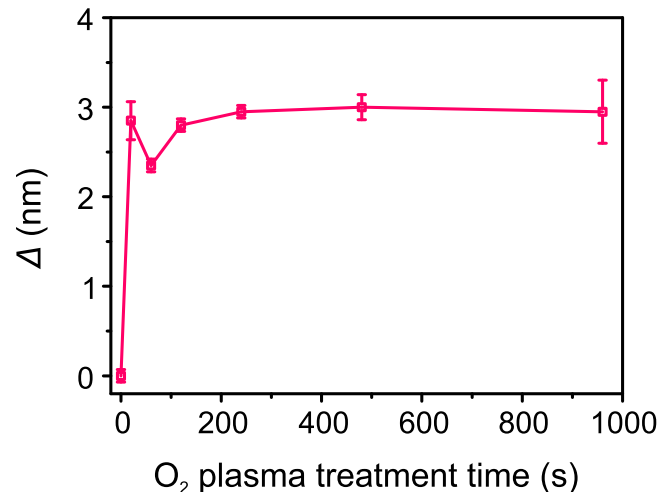


Figure 2. Thickness change of a BTS nanoplatelet as a function of oxygen plasma treatment time. The thickness values are derived from AFM height profiles.

resolution of about 0.5 cm^{-1} . An ND filter was used to reduce the light intensity and thus avoid chemical changes of the sample.

2.3. Electrical transport measurements

BTS nanoplatelets were electrically contacted in van der Pauw geometry using a Raith eLine e-beam lithography system, followed by thermal evaporation of Ti/Au (5 nm/70 nm) metal contacts. To ensure that the contacts were Ohmic, we performed Ar plasma etching of the contact areas before metal evaporation. Electrical transport measurements were performed using an AC lock-in technique in an Oxford Instruments He4 cryostat with a base temperature of 1.4 K.

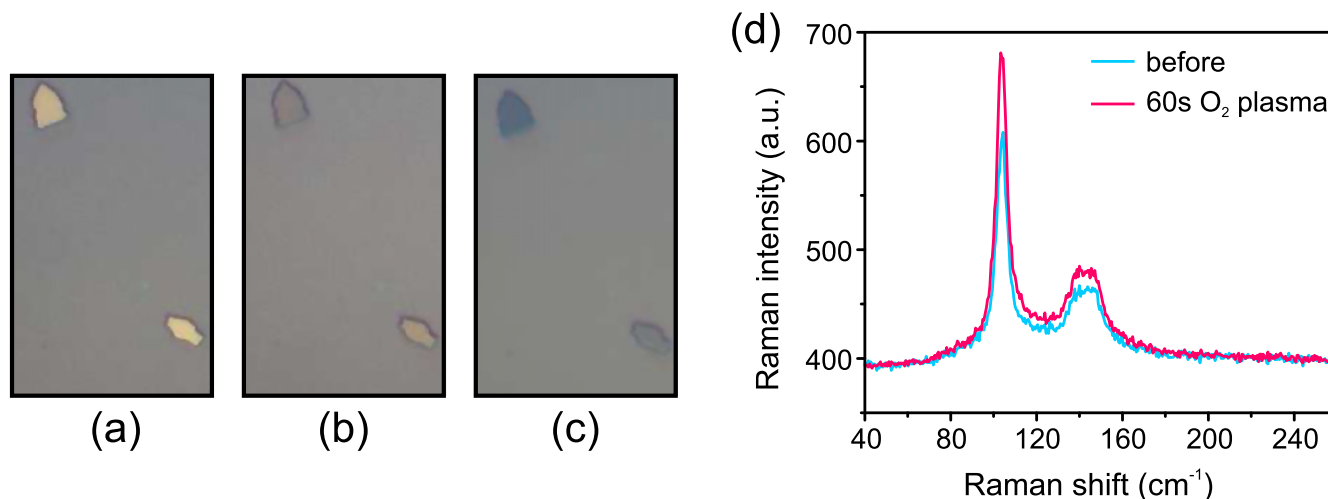


Figure 3. Optical micrographs of two BTS nanoplatelets before (a), and after 20 s (b) and 960 s (c) of oxygen plasma treatment. With increasing plasma exposure, the platelets appear more and more blue. (d) Raman spectrum of a BTS nanoplatelet before and after 60 s of oxygen plasma treatment.

3. Results and discussion

BTS nanoplatelets exposed to ambient conditions exhibited a small but detectable thickness increase over time (see figure 1), as revealed by AFM analysis of individual nanoplatelets on a Si/SiO₂ substrate.

Since the thickness of an (amorphous) oxidized quintuple layer or a layer of hydroxide exceeds the thickness of a pristine crystalline layer, the thickness increase is suitable for monitoring the oxidation process. Two regimes emerge, similar to the behavior of other bismuth chalcogenides like Bi₂Te₃ [14]. Specifically, after a pronounced initial height increase, the oxidation rate decreases after approximately 100 h, and the nanoplatelet thickness remains nearly constant up to several weeks of ambient exposure. This saturation might originate from the formation of a passivating oxide or hydroxide layer during the first stage. The maximum thickness increase on the order of 1 nm points towards the formation of an amorphous rather than a crystalline oxide or hydroxide layer, as the thickness difference between a crystalline oxidized and a non-oxidized quintuple layer is only about 0.1 nm [14], which should result in a much smaller height increase. The XPS data described below favor the formation of a hydroxide over an oxide.

Toward the aim of achieving faster oxidation which is still reproducible, we oxidized freshly grown BTS nanoplatelets by O₂ plasma. Figure 2 illustrates the thickness change for one platelet as a function of O₂ plasma treatment time (200 W at 0.3 Torr). Similar to figure 1, a fast initial increase is followed by a much lower rate approaching saturation. In the present case, the fast initial stage covers the first 20 s of plasma treatment. Additional experiments using polymer-coated nanoplatelets⁴ evidenced that the oxidation mechanism combines oxygen diffusion normal to the platelet surface with oxygen intercalation from the platelet sides. These two

processes provide a natural explanation for the observed fast initial and slow subsequent oxidation regime. In particular, once a closed surface oxide film is formed, oxidation can only continue by oxygen intercalation from the side surfaces of the platelets, which, due to their small thickness, is very slow. In total, we determined the thickness increase for more than 50 samples grown on different substrates and found an average height increase of $2.8 \text{ nm} \pm 1.7 \text{ nm}$ after 60 s. A significantly smaller variation of only 0.3 nm was observed on a certain substrate, reflecting slightly different conditions during the plasma treatments. It is noteworthy that O₂ plasma proved able to further oxidize air-exposed BTS nanoplatelets. Remarkably, even after keeping the samples in air for several weeks, subsequent O₂ plasma (60 s) still caused a thickness increase by about 1 nm.

The optical micrographs in figures 3(a)–(c) display a decrease of the optical contrast with increasing O₂ plasma treatment. This trend can be explained by a decreasing effective thickness of the crystalline BTS, while an optically transparent (and most likely amorphous) oxide is formed on top. Such correlation between optical contrast and sheet thickness goes back to interference effects, and is well-documented also for graphene and layered transition metal chalcogenides [15]. Further support for this scenario could be gained from Raman microscopy on individual nanoplatelets before and after 60 s of O₂ plasma treatment. The two representative spectra in figure 3(d) signify an intensity increase of the characteristic E_{2g} and A_{1g} Raman peaks [13] after the plasma treatment, whereas their energetic position remains unaffected. The intensity enhancement, averaged over 20 nanoplatelets, was found to be $14 \pm 7\%$. With the aid of a thickness versus Raman intensity calibration curve⁴, we determined a BTS thickness decrease of $1.85 \pm 0.95 \text{ nm}$. Combined with the AFM results, it thus follows that the oxide layer thickness is on the order of 4 nm.

In order to gain further insight into the mechanism of BTS surface oxidation and the composition of the oxide layer,

⁴ See supplemental material at (stacks.iop.org/NANO/27/285201/mmedia).

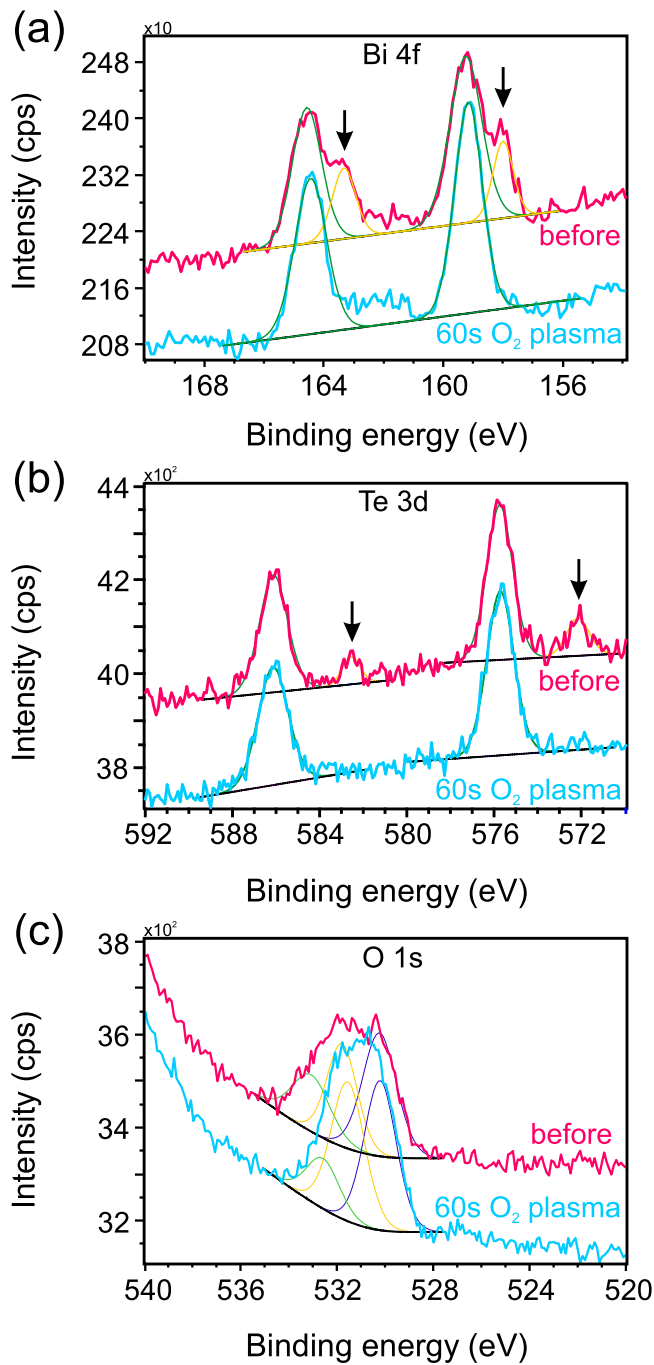


Figure 4. XPS spectra before (red) and after 60 s of oxygen plasma treatment (blue) of BTS nanoplatelets on an Au substrate, displaying the region of the Bi 4f peaks (a), the Te 3d peaks (b), as well as the O 1s peak (c).

we performed XPS measurements before and after O₂ plasma treatment (60 s). To avoid oxide signals from the Si/SiO_x substrate, the nanoplatelets were transferred onto gold-coated substrates. Before oxygen plasma treatment, signals corresponding to Bi-Te (figure 4(a); Bi 4f 7/2: 158.0 eV and figure 4(b); Te 3d 5/2: 572.2 eV) could be detected. It should be mentioned that due to the relatively low density of the nanoplatelets, the total Se concentration was below the XPS detection limit. The presence of strong Bi-O (figure 4(a); Bi

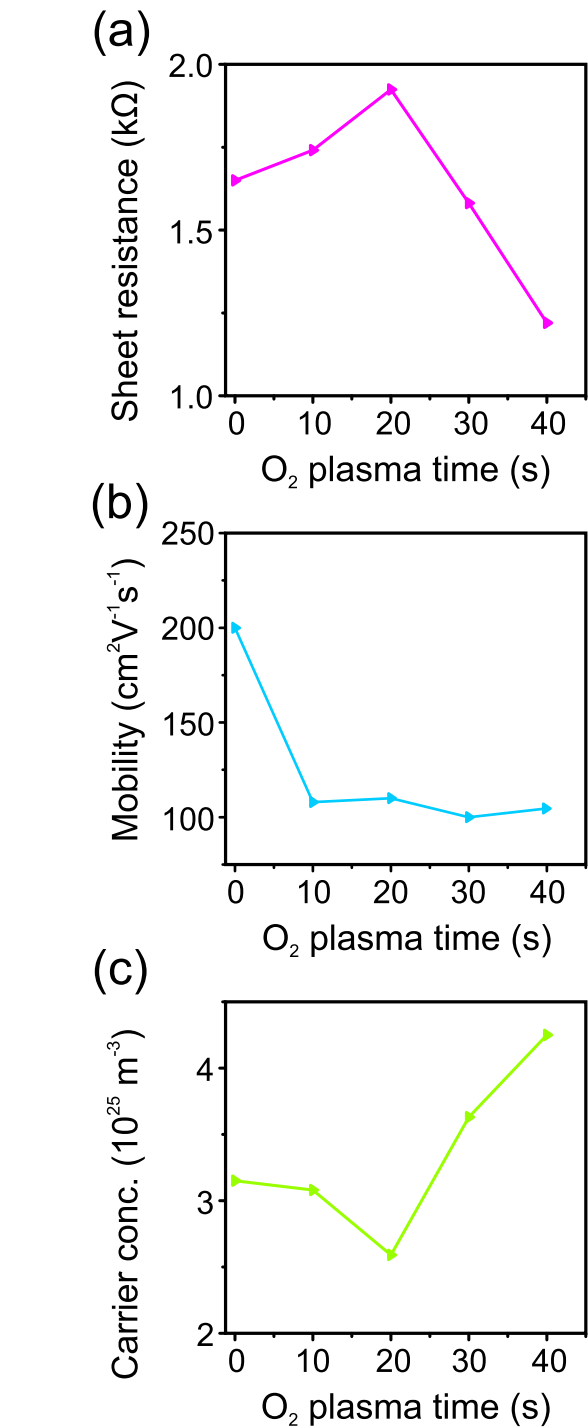


Figure 5. Sheet resistance (a), electron mobility (b), and electron concentration (c) of an individual BTS nanoplatelet subjected to different oxygen plasma treatment times. All electrical measurements were performed at low temperature ($T = 1.4$ K).

4f 7/2: 159.5 eV) and Te-O (figure 4(b); Te 3d 5/2: 576.0 eV) signals indicates partial oxidation of the nanoplatelet surface already before plasma treatment. Two different oxygen species can be distinguished, the first of which is attributable to Te-OH (figure 4(c); O 1s: 530.3 eV), while the other one corresponds to Te-O-Bi and Se-O-Bi (figure 4(c); O 1s: 532.3 eV). It thus follows that the short air exposure

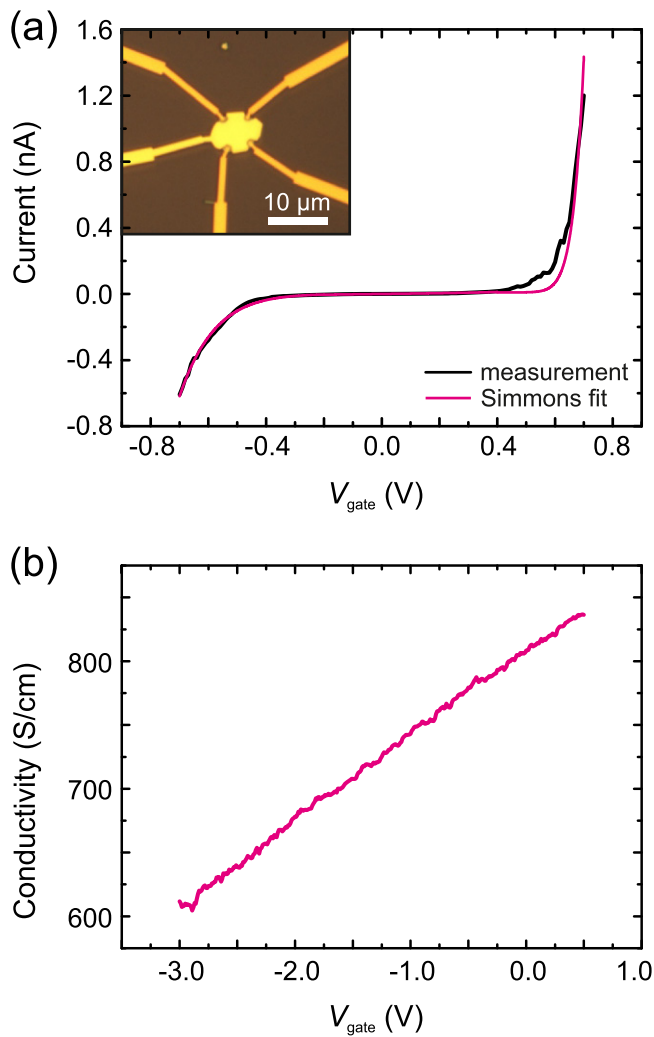


Figure 6. (a) Gate leakage characteristic of an oxygen-plasma treated BTS nanoplatelet provided with a gold top gate (see inset), recorded at room temperature. Experimental data are shown as a black line, while the red line is a data fit based upon a direct tunneling model. (b) Conductivity of a similar top-gated BTS nanoplatelet as a function of top gate voltage.

before placing the samples in the XPS chamber is sufficient to create a native oxide/hydroxide layer on the BTS surface, in agreement with our findings above (figure 1) and the reports in the literature [7, 8]. After 60 s of O_2 plasma treatment, the Bi-Te and Bi-Se signal vanished and only a Bi-O signal remained. Similarly, only a Te-O signal could be detected after plasma treatment, testifying an oxidation state change of the Te atoms near the surface from -2 to $+4$.

As the probing depth of the XPS setup is about 2 nm, it can be concluded that the BTS surface region is completely oxidized after plasma exposure. However, the presence of two oxygen signals whose intensity did not change notably upon plasma treatment strongly suggests the formation of surface hydroxyl groups upon exposure of the plasma treated BTS to ambient conditions.

Taken together, the above observations evidence a two-step oxidation process, akin to that proposed by Yashina *et al*

[7]. Air exposure first rapidly creates hydroxyl groups (Te-OH) on the top surface, followed by the slow formation of a sub-surface oxide with Bi-O-Te and Bi-O-Se bonding motifs. The major effect of oxygen plasma treatment is to enhance this oxide layer.

Recent experimental studies have suggested that the surface hydroxide on bismuth chalcogenides imparts appreciable n-type doping [16]. On this basis, the question arises whether or not the plasma-created surface oxide might have a similar doping effect. To clarify this issue, we electrically characterized individual BTS nanoplatelets. Figure 5(a) displays the evolution of sheet resistance at $T = 1.4$ K as a function of O_2 plasma treatment time. The sheet resistance first increases to a maximum at around 20 s of plasma exposure, after which it decreases again. This behavior can be understood by the combined trends of carrier mobility and concentration evolution. The carrier mobility exhibits a continuous slight decrease with increasing plasma time (see figure 5(b)), whereas the carrier concentration reaches a minimum between 30 and 60 s of plasma exposure (see figure 5(c)). The initial decrease of carrier (electron) concentration might arise from the conversion of the thin surface hydroxide to the thicker oxide, as covalently bonded oxygen on bismuth chalcogenides are known to act as p-type acceptors [17]. The subsequent electron density increase can be explained by the reduction in effective thickness. In the corresponding plot, a constant thickness d (as obtained from AFM measurements) was used to calculate the 3D carrier concentration (carriers per volume). However, if the BTS thickness decreases, according to $n = BR_H/(qd)$, where B , R_H and q are the magnetic field, the Hall-constant and the elementary charge, respectively, the carrier concentration n effectively increases. It follows that the O_2 plasma treatment reduces both the degree of n-doping and the effective thickness of the BTS nanoplatelets. Since it is expected that the bottom side of the nanoplatelets, which is in contact with the substrate, is well protected from external influences [23] like oxidation, the plasma induced doping will mainly influence the top surface and bulk of the material.

As another indicator of the structural integrity of the plasma-generated oxide on the BTS, we evaluated its electrical insulating capability by adding a gold contact (Ti/Au, 2 nm/30 nm) on top of the nanoplatelets. In figure 6(a), low temperature ($T = 1.4$ K) I - V characteristics recorded between the top gate and the source contact of a BTS platelet are shown. For nanoplatelets subjected to 60 s of O_2 plasma treatment, the gate leakage curves of the metal-oxide-BTS-metal structures exhibit a low-bias resistance of several G Ω .

Assuming an oxide thickness of 2 nm, the I - V curves can be well-fitted using a semi-empirical equation for direct tunneling [18]. The fits yield an estimate of 2 eV for the tunneling barrier height, which is in reasonable agreement with values reported for common oxide gate dielectrics [19].

Furthermore, the plot in figure 6(b) exemplifies that the structural quality of the oxide is sufficient for electrostatic gating of the nanoplatelets, as apparent from the monotonous increase of conductivity upon sweeping from positive to negative top-gate voltages. However, the achievable

conductance modulation on the order of tens of per cent indicates inferior gate performance, as compared to top-gates combined with a high-k dielectric insulator like HfO₂ or Al₂O₃ [20]. This difference can be attributed to the suppression of direct tunneling through such 20 nm thick oxide films.

4. Conclusion

In summary, we have demonstrated that oxygen plasma treatment of BTS nanoplatelets leads to the formation of a compact, few nm thick surface oxide layer. Similar to the surface hydroxyl groups formed during oxidation under ambient conditions, the oxide layer imparts p-type doping, thus reducing the electron density in the material. The resistance of the platelets is only weakly affected, with a resistance maximum occurring as a function of plasma time, which is attributable to the combined effect of enhanced p-doping and decreased platelet thickness. Although the surface oxide is in principle able to serve as a gate dielectric below a top gate, its leakage characteristic needs to be further improved to enable useful gate modulation.

Acknowledgments

The authors acknowledge the help of M Konuma with the XPS measurements.

References

- [1] Fu L and Kane C L 2007 *Phys. Rev. B* **76** 045302
- [2] Moore J E 2010 *Nature* **464** 194
- [3] Hsieh D, Qian D, Wray L, Xia Y, Hor Y S, Cava R and Hasan M Z 2008 *Nature* **452** 970
- [4] Hu D H, Vishik I M, Yi M, Chen Y L, Moore R G and Shen Z X 2012 *Annu. Rev. Condens. Matter Phys.* **3** 129
- [5] Xia Y *et al* 2009 *Nat. Phys.* **5** 398
- [6] Analytis J G, Chu J-H, Chen Y, Corredor F, McDonald R D, Shen Z and Fisher I R 2010 *Phys. Rev. B* **81** 205407
- [7] Yashina L V *et al* 2013 *ACS Nano* **7** 5181
- [8] Kong D S *et al* 2011 *ACS Nano* **5** 4698
- [9] Hsieh D, McIver J W, Torchinsky D H, Gardner D R, Lee Y S and Gedik N 2011 *Phys. Rev. Lett.* **106** 057401
- [10] Hong S S, Kundhikanjana W, Cha J J, Lai K J, Kong D S, Meister S, Kelly M A, Shen Z X and Cui Y 2010 *Nano Lett.* **10** 3118
- [11] Taskin A A, Ren Z, Sasaki S, Segawa K and Ando Y 2011 *Phys. Rev. Lett.* **107** 016801
- [12] Hwang J H, Park J, Kwon S, Kim J S and Park J J 2014 *Surf. Sci.* **630** 153
- [13] Gehring P, Gao B, Burghard M and Kern K 2012 *Appl. Phys. Lett.* **101** 023116
- [14] Bando H, Koizumi K, Oikawa Y, Daikohara K, Kulbachinskii V A and Ozaki H 2000 *J. Phys. Cond. Mat.* **12** 5607
- [15] Ni Z H, Wang H M, Kasim J, Fan H M, Yu T, Wu Y H, Feng Y P and Shen Z X 2007 *Nano Lett.* **7** 2758
- [16] Benia H M, Lin C T, Kern K and Ast C R 2011 *Phys. Rev. Lett.* **107** 177602
- [17] McIver W, Hsieh D, Drapcho S G, Torchinsky D H, Gardner D H, Lee Y S and Gedik N 2012 *Phys. Rev. B* **86** 035327
- [18] Yeo Y-C, King T-J and Hu C 2002 *Appl. Phys. Lett.* **81** 2091
- [19] Wu W C, Lai C S, Wang T M, Wang J C, Hsu C W, Ma M W and Chao T S 2008 *Electrochem. Solid-State Lett.* **11** H15
- [20] Steinberg H, Gardner D R, Lee Y S and Jarillo-Herreo P 2010 *Nano Lett.* **10** 5032
- [21] Gehring P, Gao B, Burghard M and Kern K 2012 *Nano Lett.* **12** 5137
- [22] Vaklinova K, Hoyer A, Burghard M and Kern K 2016 *Nano Lett.* **16** 2595–602
- [23] Li Z *et al* 2015 *Phys. Rev. B* **91** 041401 (R)